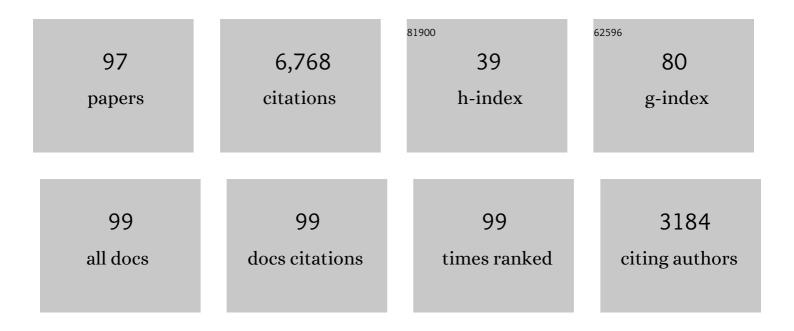
Yingjie Yang

List of Publications by Year in descending order

Source: https://exaly.com/author-pdf/2924372/publications.pdf Version: 2024-02-01



YINCHE YANG

#	Article	IF	CITATIONS
1	Processing seismic ambient noise data to obtain reliable broad-band surface wave dispersion measurements. Geophysical Journal International, 2007, 169, 1239-1260.	2.4	1,705
2	Ambient noise Rayleigh wave tomography across Europe. Geophysical Journal International, 2007, 168, 259-274.	2.4	486
3	A synoptic view of the distribution and connectivity of the mid rustal low velocity zone beneath Tibet. Journal of Geophysical Research, 2012, 117, .	3.3	214
4	Characteristics of ambient seismic noise as a source for surface wave tomography. Geochemistry, Geophysics, Geosystems, 2008, 9, .	2.5	212
5	Seismic evidence for widespread western-US deep-crustal deformation caused by extension. Nature, 2010, 464, 885-889.	27.8	178
6	Structure of the crust and uppermost mantle beneath the western United States revealed by ambient noise and earthquake tomography. Journal of Geophysical Research, 2008, 113, .	3.3	175
7	Regional tomographic inversion of the amplitude and phase of Rayleigh waves with 2-D sensitivity kernels. Geophysical Journal International, 2006, 166, 1148-1160.	2.4	174
8	The structure of the crust and uppermost mantle beneath South China from ambient noise and earthquake tomography. Geophysical Journal International, 2012, 189, 1565-1583.	2.4	166
9	Complex and variable crustal and uppermost mantle seismic anisotropy in the western UnitedÂStates. Nature Geoscience, 2011, 4, 55-61.	12.9	151
10	Crust and uppermost mantle beneath the North China Craton, northeastern China, and the Sea of Japan from ambient noise tomography. Journal of Geophysical Research, 2011, 116, .	3.3	134
11	Rayleigh wave phase velocities, small-scale convection, and azimuthal anisotropy beneath southern California. Journal of Geophysical Research, 2006, 111, .	3.3	133
12	On the limitations of interstation distances in ambient noise tomography. Geophysical Journal International, 2015, 201, 652-661.	2.4	127
13	Crustal radial anisotropy across Eastern Tibet and the Western Yangtze Craton. Journal of Geophysical Research: Solid Earth, 2013, 118, 4226-4252.	3.4	126
14	3â€D multiobservable probabilistic inversion for the compositional and thermal structure of the lithosphere and upper mantle. I: <i>a priori</i> petrological information and geophysical observables. Journal of Geophysical Research: Solid Earth, 2013, 118, 2586-2617.	3.4	121
15	Surface wave tomography of China from ambient seismic noise correlation. Geochemistry, Geophysics, Geosystems, 2008, 9, .	2.5	111
16	Seismic evidence of on-going sublithosphere upper mantle convection for intra-plate volcanism in Northeast China. Earth and Planetary Science Letters, 2016, 433, 31-43.	4.4	107
17	A 3-D shear velocity model of the crust and uppermost mantle beneath the United States from ambient seismic noise. Geophysical Journal International, 2009, 177, 1177-1196.	2.4	105
18	Rayleigh wave phase velocity maps of Tibet and the surrounding regions from ambient seismic noise tomography. Geochemistry, Geophysics, Geosystems, 2010, 11, .	2.5	105

#	Article	IF	CITATIONS
19	Crustal and uppermost mantle structure in southern Africa revealed from ambient noise and teleseismic tomography. Geophysical Journal International, 2008, 174, 235-248.	2.4	97
20	Crustal shear wave velocity structure of the western United States inferred from ambient seismic noise and earthquake data. Journal of Geophysical Research, 2010, 115, .	3.3	94
21	Seismic attenuation near the East Pacific Rise and the origin of the low-velocity zone. Earth and Planetary Science Letters, 2007, 258, 260-268.	4.4	85
22	Local modification of the lithosphere beneath the central and western North China Craton: 3-D constraints from Rayleigh wave tomography. Gondwana Research, 2013, 24, 849-864.	6.0	84
23	Ambient noise surface wave tomography of the Iberian Peninsula: Implications for shallow seismic structure. Geophysical Research Letters, 2007, 34, .	4.0	80
24	3â€D multiâ€observable probabilistic inversion for the compositional and thermal structure of the lithosphere and upper mantle. II: General methodology and resolution analysis. Journal of Geophysical Research: Solid Earth, 2013, 118, 1650-1676.	3.4	78
25	Penetration of mid-crustal low velocity zone across the Kunlun Fault in the NE Tibetan Plateau revealed by ambient noise tomography. Earth and Planetary Science Letters, 2014, 406, 81-92.	4.4	75
26	Crustal structure beneath the Dabie orogenic belt from ambient noise tomography. Earth and Planetary Science Letters, 2012, 313-314, 12-22.	4.4	73
27	3â€D multiobservable probabilistic inversion for the compositional and thermal structure of the lithosphere and upper mantle: III. Thermochemical tomography in the Westernâ€Central U.S Journal of Geophysical Research: Solid Earth, 2016, 121, 7337-7370.	3.4	67
28	Rayleigh wave tomography beneath intraplate volcanic ridges in the South Pacific. Journal of Geophysical Research, 2007, 112, .	3.3	64
29	Rayleigh wave tomography of the northeastern margin of the Tibetan Plateau. Earth and Planetary Science Letters, 2011, 304, 103-112.	4.4	62
30	Three dimensional shear wave velocity structure of the crust and upper mantle beneath China from ambient noise surface wave tomography. Earthquake Science, 2010, 23, 449-463.	0.9	54
31	Thermochemical structure of the North China Craton from multi-observable probabilistic inversion: Extent and causes of cratonic lithosphere modification. Gondwana Research, 2016, 37, 252-265.	6.0	54
32	Crustal and uppermost mantle velocity structure and its relationship with the formation of ore districts in the Middle–Lower Yangtze River region. Earth and Planetary Science Letters, 2014, 408, 378-389.	4.4	53
33	The Origin and Mantle Dynamics of Quaternary Intraplate Volcanism in Northeast China From Joint Inversion of Surface Wave and Body Wave. Journal of Geophysical Research: Solid Earth, 2018, 123, 2410-2425.	3.4	50
34	Teleseismic surface wave tomography in the western U.S. using the Transportable Array component of USArray. Geophysical Research Letters, 2008, 35, .	4.0	49
35	Crustal radial anisotropy beneath the Dabie orogenic belt from ambient noise tomography. Geophysical Journal International, 2013, 195, 1149-1164.	2.4	49
36	The thermochemical structure of the lithosphere and upper mantle beneath south China: Results from multiobservable probabilistic inversion. Journal of Geophysical Research: Solid Earth, 2014, 119, 8417-8441.	3.4	45

#	Article	IF	CITATIONS
37	Mantle heterogeneity and off axis volcanism on young Pacific lithosphere. Earth and Planetary Science Letters, 2011, 311, 306-315.	4.4	42
38	Crustal structure determined from ambient noise tomography near the magmatic centers of the Coso region, southeastern California. Geochemistry, Geophysics, Geosystems, 2011, 12, n/a-n/a.	2.5	40
39	Crustal and upper mantle structure and the deep seismogenic environment in the source regions of the Lushan earthquake and the Wenchuan earthquake. Science China Earth Sciences, 2013, 56, 1158-1168.	5.2	40
40	Crustal structure of the northeastern Tibetan plateau, the Ordos block and the Sichuan basin from ambient noise tomography. Earthquake Science, 2010, 23, 465-476.	0.9	39
41	Measurement of Rayleigh wave ellipticity and its application to the joint inversion of highâ€resolution <i>S</i> wave velocity structure beneath northeast China. Journal of Geophysical Research: Solid Earth, 2016, 121, 864-880.	3.4	38
42	Improving Epicentral and Magnitude Estimation of Earthquakes from T Phases by Considering the Excitation Function. Bulletin of the Seismological Society of America, 2003, 93, 2106-2122.	2.3	36
43	Attenuation in the upper mantle beneath Southern California: Physical state of the lithosphere and asthenosphere. Journal of Geophysical Research, 2008, 113, .	3.3	34
44	Crustal velocity structure of Central and Eastern Turkey from ambient noise tomography. Geophysical Journal International, 2013, 194, 1941-1954.	2.4	33
45	Title is missing!. , 2012, 8, 1310.		28
46	How did the Dabie Orogen collapse? Insights from 3â€Ð magnetotelluric imaging of profile data. Journal of Geophysical Research: Solid Earth, 2016, 121, 5169-5185.	3.4	28
47	Refined crustal and uppermost mantle structure of southern California by ambient noise adjoint tomography. Geophysical Journal International, 2018, 215, 844-863.	2.4	28
48	Lithospheric Structure of the Northern Ordos From Ambient Noise and Teleseismic Surface Wave Tomography. Journal of Geophysical Research: Solid Earth, 2018, 123, 6940-6957.	3.4	27
49	Crust and upper mantle structure beneath southeast Australia from ambient noise and teleseismic tomography. Tectonophysics, 2016, 689, 143-156.	2.2	26
50	Seismological Evidence for a Remnant Oceanic Slab in the Western Junggar, Northwest China. Journal of Geophysical Research: Solid Earth, 2018, 123, 4157-4170.	3.4	26
51	An investigation of time–frequency domain phase-weighted stacking and its application to phase-velocity extraction from ambient noise's empirical Green's functions. Geophysical Journal International, 2018, 212, 1143-1156.	2.4	25
52	Application of teleseismic long-period surface waves from ambient noise in regional surface wave tomography: a case study in western USA. Geophysical Journal International, 2014, 198, 1644-1652.	2.4	24
53	Crustal Deformation in Southern California Constrained by Radial Anisotropy From Ambient Noise Adjoint Tomography. Geophysical Research Letters, 2020, 47, e2020GL088580.	4.0	24
54	Improving cross-correlations of ambient noise using an rms-ratio selection stacking method. Geophysical Journal International, 2020, 222, 989-1002.	2.4	23

#	Article	IF	CITATIONS
55	Surface wave tomography on a large-scale seismic array combining ambient noise and teleseismic earthquake data. Earthquake Science, 2011, 24, 55-64.	0.9	22
56	Crustal structure in the junction of Qinling Orogen, Yangtze Craton and Tibetan Plateau: implications for the formation of the Dabashan Orocline and the growth of Tibetan Plateau. Geophysical Journal International, 2016, 205, 1670-1681.	2.4	22
57	Crustal radial anisotropy in Northeast China and its implications for the regional tectonic extension. Geophysical Journal International, 2016, 207, 197-208.	2.4	21
58	Epicentral location based on Rayleigh wave Empirical Green's Functions from ambient seismic noise. Geophysical Journal International, 2011, 184, 869-884.	2.4	19
59	Lithosphere–asthenosphere interactions beneath northeast China and the origin of its intraplate volcanism. Geology, 2022, 50, 210-215.	4.4	19
60	The uppermost mantle seismic velocity structure of West Antarctica from Rayleigh wave tomography: Insights into tectonic structure and geothermal heat flow. Earth and Planetary Science Letters, 2019, 522, 219-233.	4.4	18
61	The Deep Lithospheric Structure of the Junggar Terrane, NW China: Implications for Its Origin and Tectonic Evolution. Journal of Geophysical Research: Solid Earth, 2019, 124, 11615-11638.	3.4	18
62	Threeâ€Dimensional Sensitivity Kernels for Multicomponent Empirical Green's Functions From Ambient Noise: Methodology and Application to Adjoint Tomography. Journal of Geophysical Research: Solid Earth, 2019, 124, 5794-5810.	3.4	17
63	Coupled seismic slip on adjacent oceanic transform faults. Geophysical Research Letters, 2003, 30, .	4.0	16
64	The crustal structure of the <scp>A</scp> rizona <scp>T</scp> ransition <scp>Z</scp> one and southern <scp>C</scp> olorado <scp>P</scp> lateau from multiobservable probabilistic inversion. Geochemistry, Geophysics, Geosystems, 2016, 17, 4308-4332.	2.5	16
65	Correction of phase velocity bias caused by strong directional noise sources in high-frequency ambient noise tomography: a case study in Karamay, China. Geophysical Journal International, 2016, 205, 715-727.	2.4	15
66	Evaluating Uncertainties of Phase Velocity Measurements from Cross-Correlations of Ambient Seismic Noise. Seismological Research Letters, 2020, 91, 1717-1729.	1.9	15
67	Unraveling overtone interferences in Love-wave phase velocity measurements by radon transform. Geophysical Journal International, 2015, 203, 327-333.	2.4	14
68	Crustal structure of the Newer Volcanics Province, SE Australia, from ambient noise tomography. Tectonophysics, 2016, 683, 382-392.	2.2	13
69	Physical State and Structure of the Crust Beneath the Westernâ€Central United States From Multiobservable Probabilistic Inversion. Tectonics, 2018, 37, 3117-3147.	2.8	13
70	Thermochemical State of the Upper Mantle Beneath South China From Multiâ€Observable Probabilistic Inversion. Journal of Geophysical Research: Solid Earth, 2021, 126, e2020JB021114.	3.4	12
71	High-resolution lithospheric structures of the Qinling-Dabie orogenic belt: Implications for deep subduction and delamination of continental lithosphere. Tectonophysics, 2021, 806, 228799.	2.2	12
72	Thermochemical structure and evolution of cratonic lithosphere in central and southern Africa. Nature Geoscience, 2022, 15, 405-410.	12.9	12

#	Article	IF	CITATIONS
73	3-D Upper-Mantle Shear Velocity Model Beneath the Contiguous United States Based on Broadband Surface Wave from Ambient Seismic Noise. Pure and Applied Geophysics, 2018, 175, 3403-3418.	1.9	11
74	Joint Inversion of Rayleigh Wave Phase Velocity, Particle Motion, and Teleseismic Body Wave Data for Sedimentary Structures. Geophysical Research Letters, 2019, 46, 6469-6478.	4.0	11
75	Mapping Crustal Shear Wave Velocity Structure and Radial Anisotropy Beneath West Antarctica Using Seismic Ambient Noise. Geochemistry, Geophysics, Geosystems, 2019, 20, 5014-5037.	2.5	10
76	Crustal Radial Anisotropy of the Iran Plateau Inferred From Ambient Noise Tomography. Journal of Geophysical Research: Solid Earth, 2021, 126, e2020JB020236.	3.4	10
77	Adjoint Tomography of Ambient Noise Data and Teleseismic P Waves: Methodology and Applications to Central California. Journal of Geophysical Research: Solid Earth, 2021, 126, e2021JB021648.	3.4	10
78	Broadband Finite Frequency Ambient Noise Tomography: A Case Study in the Western United States Using USArray Stations. Journal of Geophysical Research: Solid Earth, 2020, 125, e2019JB019314.	3.4	10
79	Constructing shear velocity models from surface wave dispersion curves using deep learning. Journal of Applied Geophysics, 2022, 196, 104524.	2.1	10
80	Seismic imaging of the Caosiyao giant porphyry molybdenum deposit using ambient noise tomography. Geophysics, 2021, 86, B401-B412.	2.6	9
81	Calibration of an Integrated Robotic Multimodal Range Scanner. IEEE Transactions on Instrumentation and Measurement, 2006, 55, 1148-1159.	4.7	8
82	On the accuracy of long-period Rayleigh waves extracted from ambient noise. Geophysical Journal International, 2016, 206, 48-55.	2.4	8
83	Effects of shallow density structure on the inversion for crustal shear wave speeds in surface wave tomography. Geophysical Journal International, 2016, 205, 1144-1152.	2.4	8
84	Threeâ€Ðimensional Crustal Structures of the Shanxi Rift Constructed by Rayleigh Wave Dispersion Curves and Ellipticity: Implication for Sedimentation, Intraplate Volcanism, and Seismicity. Journal of Geophysical Research: Solid Earth, 2020, 125, e2020JB020146.	3.4	8
85	The deep thermochemical structure of the Dabie orogenic belt from multi-observable probabilistic inversion. Tectonophysics, 2020, 787, 228478.	2.2	8
86	3â€Ð Sedimentary Structures Beneath Southeastern Australia Constrained by Passive Seismic Array Data. Journal of Geophysical Research: Solid Earth, 2021, 126, e2020JB019998.	3.4	6
87	New Insights Into Potassic Intraplate Volcanism in Northeast China From Joint Tomography of Ambient Noise and Teleseismic Surface Waves. Journal of Geophysical Research: Solid Earth, 2021, 126, e2021JB021856.	3.4	6
88	Full-Waveform Inversion of High-Frequency Teleseismic Body Waves Based on Multiple Plane-Wave Incidence: Methods and Practical Applications. Bulletin of the Seismological Society of America, 2022, 112, 118-132.	2.3	6
89	Joint Inversion of Active Sources and Ambient Noise for Near‧urface Structures: A Case Study in the Balikun Basin, China. Seismological Research Letters, 2018, , .	1.9	5
90	3D imaging of the Earth's lithosphere using noise from ocean waves. ASEG Extended Abstracts, 2016, 2016. 1-5.	0.1	5

#	Article	IF	CITATIONS
91	Seismic Imaging of a Magma Chamber and Melt Recharge of the Dormant Datong Volcanoes. Earth and Space Science, 2021, 8, e2021EA001931.	2.6	5
92	Metallogenic potential of the Wulong goldfield, Liaodong Peninsula, China revealed by high-resolution ambient noise tomography. Ore Geology Reviews, 2022, 142, 104704.	2.7	4
93	Extracting surface wave dispersion curves from asynchronous seismic stations: method and application. Geophysical Journal International, 2021, 226, 1148-1158.	2.4	3
94	Eastward Asthenospheric Flow From NE Tibet Inferred by Joint Inversion of Teleseismic Body and Surface Waves: Insight Into Widespread Continental Deformation in Eastern China. Journal of Geophysical Research: Solid Earth, 2022, 127, .	3.4	3
95	Retrieving PmP Travel Times From a Persistent Localized Microseismic Source. Geophysical Research Letters, 2021, 48, e2021GL094827.	4.0	2
96	Full Waveform Ambient Noise Tomography for the Northern Mississippi Embayment. Journal of Geophysical Research: Solid Earth, 2022, 127, .	3.4	2
97	A Broadband Seismic Network in the Middle-Lower Yangtze Metallogenic Belt, China. Seismological Research Letters, 2015, 86, 941-947.	1.9	0